Physics of Plasmas

Evidence on the effects of main-chamber neutrals on density shoulder broadening

Cite as: Phys. Plasmas **29**, 062507 (2022); https://doi.org/10.1063/5.0090260
Submitted: 04 March 2022 • Accepted: 01 June 2022 • Published Online: 14 June 2022

C. K. Tsui, J. A. Boedo, D. Brida, et al.

Physics of Plasmas ARTICLE scitation.org/journal/php

Evidence on the effects of main-chamber neutrals on density shoulder broadening

Cite as: Phys. Plasmas **29**, 062507 (2022); doi: 10.1063/5.0090260
Submitted: 4 March 2022 · Accepted: 1 June 2022 ·
Published Online: 14 June 2022

C. K. Tsui,[1,a)] J. A. Boedo,[1] D. Brida,[2] O. Février,[3] G. F. Harrer,[4] A. Perek,[5] H. Reimerdes,[3] B. P. Duval,[3] S. Gorno,[3] U. A. Sheikh,[3] C. Theiler,[3] N. Vianello,[6] N. Walkden,[7] M. Wensing,[2] M. Baquero-Ruiz,[2] TCV Team[b)] and MST1 Team[c)]

AFFILIATIONS

[1]Center for Energy Research, University of California San Diego (UCSD), La Jolla, California 92093, USA
[2]Max Planck Institute for Plasma Physics, Boltzmannstraße 2, 85748 Garching, Germany
[3]École Polytechnique Fédérale de Lausanne (EPFL), Swiss Plasma Center (SPC), Lausanne CH-1015, Switzerland
[4]Institute of Applied Physics, TU Wien, Fusion@ÖAW, Wiedner Hauptstr. 8-10, 1040 Vienna, Austria
[5]Dutch Institute for Fundamental Energy Research, De Zaale 20, 5612 AJ Eindhoven, Netherlands
[6]Consorzio RFX (CNR, ENEA, INFN, Universitá di Padova, Acciaierie Venete SpA), Corso Stati Uniti 4, 35127 Padova, Italy
[7]CCFE, Culham Science Centre, Abingdon OX14 3DB, United Kingdom

[a)]**Author to whom correspondence should be addressed:** C7tsui@UCSD.edu
[b)]See the author list of Coda *et al.*, Nucl. Fusion **59**, 112023 (2019).
[c)]See author list of Labit *et al.*, Nucl. Fusion **59**, 086020 (2019).

ABSTRACT

Evidence that density shoulder broadening is dependent on high main-chamber neutral density is presented. Shoulder broadening does not occur when the sources for main-chamber neutrals are minimized using divertor baffles and wide gaps to the first wall ($\sim 3\times$ the density decay length). Removing the baffles or reducing the gap to the inner wall both act to increase the density shoulder amplitude in otherwise identical TCV discharges. Radial turbulent transport is correlated with shoulder amplitude.

I. INTRODUCTION

Scrape-off layers (SOL) in tokamaks often exhibit a two-layer structure with a steep density decay length close to the separatrix and a longer one in the far-SOL.[1,2] This structure called the "density shoulder" cannot be modeled using radially constant cross field diffusion coefficients, nor with combinations of constant diffusive and convective transport coefficients.[3–6] Far-SOL density profiles have been observed to broaden with increasing divertor collisionality,[1,2,7–11] increasing the plasma density at the first wall by up to an order of magnitude. This makes the prediction of main chamber plasma flux highly uncertain for future devices and even for current tokamaks. This uncertainty also precludes accurate predictions of main-chamber recycling (with implications for core fueling and density control), main chamber erosion, impurity sputtering, dust generation, and the first wall lifespan.

Many studies[7,8,12–18] support the link between filamentary transport and density shoulder formation when the normalized collisionality $\Lambda > 1$. (Λ is described in Refs. 19 and 20, and below.) However, impurity seeding experiments have shown that high Λ is not sufficient by itself to guarantee shoulder formation,[16,17,21–24] indicating that our understanding is incomplete.

Therefore, alternative mechanisms for shoulder formation must be considered. One hypothesis[2,16] is that high main-chamber neutral pressure drives density shoulder formation by increasing upstream ionization rates. High main-chamber neutral density may also increase radial turbulent transport by dampening zonal flows,[25] or by increasing filamentary transport via inter-filament ionization.[26,27] Another possibility is that changes in the plasma sink to the target is the primary mechanism controlling shoulder formation. Changes in divertor geometry in JET affected shoulder amplitude without changing midplane neutral pressure, while a strong correlation between divertor Dα intensity and shoulder amplitude was observed.[22] Modeling using the GBS turbulence code shows that increased divertor ionization can cool the divertor, reducing the parallel flux toward the targets.[28] Particle

balance indicated that it was the reduction in the sink term rather than changes in turbulent transport which caused the density shoulder broadening.[28]

II. EXPERIMENTAL SETUP

Ohmic L-mode density ramps were performed with and without baffles with $B \times \nabla B$ pointing upward (unfavorable for H-mode). Shape, Ip = −340 kA, and Bt = 1.4 T were held constant. The main-chamber neutral density was modified using the divertor baffles, which are extended graphite tiles that separate the vessel into the main and divertor chambers[29,30] as shown by the green area in Fig. 1. The main-chamber neutral density was further modified by changing the inner wall gap, which is where the SOL flux surfaces first intersect the wall outside of the divertor. This provides four scenarios with the shot numbers listed in Fig. 1.

The "large gap" scenarios have 3.6 cm between the separatrix and the inner wall, which is R_{wall}-R_{sep} = 2.3 cm when mapped to the outer midplane (OMP) or ∼3× the density decay length $\lambda_{ne,near}$. The "small gap" scenarios have a 2.0 cm inner gap, which is R_{wall}-R_{sep} = 1.2 cm or ∼1.5× $\lambda_{ne,near}$. The first flux surface to intersect the outer baffle has R-R_{sep} = 2.7 cm, and the first to intersect the outer wall has R-R_{sep} > 4.5 cm (i.e., the gap between the separatrix and the outer wall is at least 4.5 cm).

In addition to the four nearly identical examples, reciprocating probe plunges were collected from similar discharges to make an expanded database. Variations in I_p of up to 10% and small changes in shape were permitted. Only discharges which fit into the baffled large gap (green) and unbaffled small gap (red) categories were included. The additional unbaffled small gap cases have R_{wall}-R_{sep} ≤ 1.2 cm, and the additional baffled large gap cases have R_{wall}-R_{sep} > 2.0 cm.

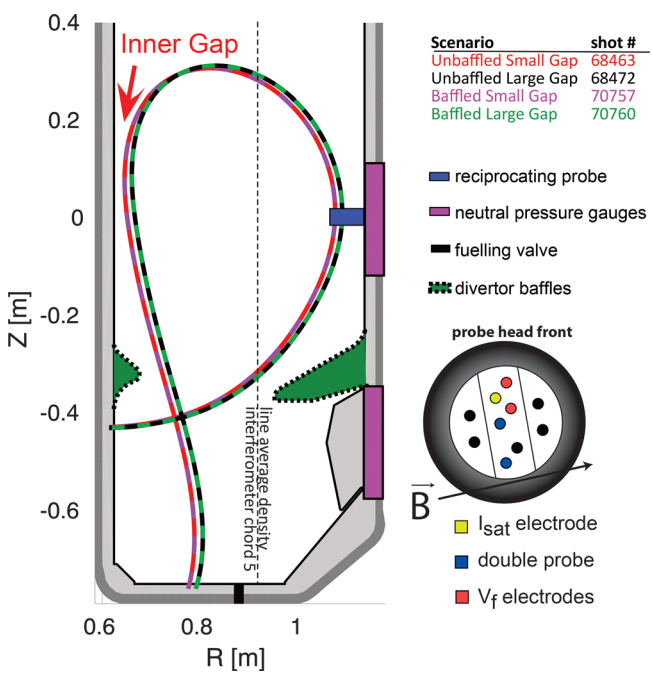

FIG. 1. A poloidal cross section of TCV with the separatrix of the four scenarios. The outline of the baffles (when present) is shown by the green area. The locations of the primary diagnostics are shown in the legend. Inset on the bottom right is a diagram of the reciprocating probe head and the electrodes used in the current study.

The locations of the reciprocating probe measurements and the fueling valve are shown in Fig. 1, left. Capacitance monometers were used to measure the neutral pressure in a midplane port (upper magenta rectangle) and in the lower duct ahead of a turbo molecular pump (lower magenta rectangle). The turbopump reduced the pressure measurements by a constant ∼30% compared to when the pump duct was closed in tests with no plasma.

Reciprocating probe electrodes are labeled based on their function in Fig. 1, right. The electron temperature T_e was measured using the "double probe" electrodes, electron density n_e, and its fluctuating component $\tilde{n}_e$ were calculated using the saturation current from the "I_{sat} electrode." The electrode collection area was calculated as a function of I_{sat} and T_e accounting for Debye sheath expansion and finite Larmor radius.[31] The floating potential V_f and the fluctuating component of the poloidal electric field $\tilde{E}_\theta$ were estimated from the two "V_f electrodes." The radial turbulent flux to be determined using[32]

$$\Gamma_r^{turb} = \frac{\langle \tilde{n}_e \tilde{E}_\theta \rangle}{B_t}, \tag{1}$$

where the angled brackets indicate a time average over 2 ms intervals. Fluctuating quantities were sampled at 10 MHz.

III. DIVERTOR CLOSURE EFFECTS

The effects of divertor closure on divertor conditions have been investigated at length,[29,30,33–38] and are only summarized here. Figure 2 shows the evolution of the divertor conditions as a function of the line-averaged density $\langle n_e \rangle$ for the four scenarios.

The outer target I_{sat} rollover [Fig. 2(a)] occurs earlier [at lower $\langle n_e \rangle$] and more deeply for the baffled discharges confirming that the baffles provide improved access to detached conditions.[33,34] This is consistent with Fig. 2(b) which shows that the baffled divertor plasmas are colder and denser with higher normalized divertor collisionality Λ_{div}. This estimate was formulated in Ref. 20 and refined in Ref. 8 to use plasma conditions measured at the target since the changes in collisionality near the onset of detachment are stonger in the divertor:

$$\Lambda \sim \Lambda_{div} = 1.7 \times 10^{-14} \frac{n_e L_{||}^{div}}{T_e^2}, \tag{2}$$

where $L_{||}^{div}$ (cm) is the connection length from the target to the X-point region, n_e (cm^{-3}) is the electron density, and T_e (eV) is the electron temperature obtained from the outer-target Langmuir Probes.[39,40] Since Λ_{div} varies with R-R_{sep}, the median is taken to provide a representative value for the outer target.

Λ_{div} [Fig. 2(b)] is between 3 and 25 for all scenarios, i.e., in the range of the "Resistive X-point regime," where filamentary transport is expected to increase with collisionality[19,20] and where strong density shoulders have previously been observed in unseeded TCV discharges.[3,14,17,23] Λ_{div} increases with $\langle n_e \rangle$ and is consistently higher for the baffled scenarios than the unbaffled ones. Detailed target profiles of n_e and T_e as a function of $\langle n_e \rangle$ for similar plasma conditions are available in Ref. 33.

The divertor neutral pressure [Fig. 2(c)] is ∼2–3× higher for the baffled scenarios consistent with previous measurements[33,34] and

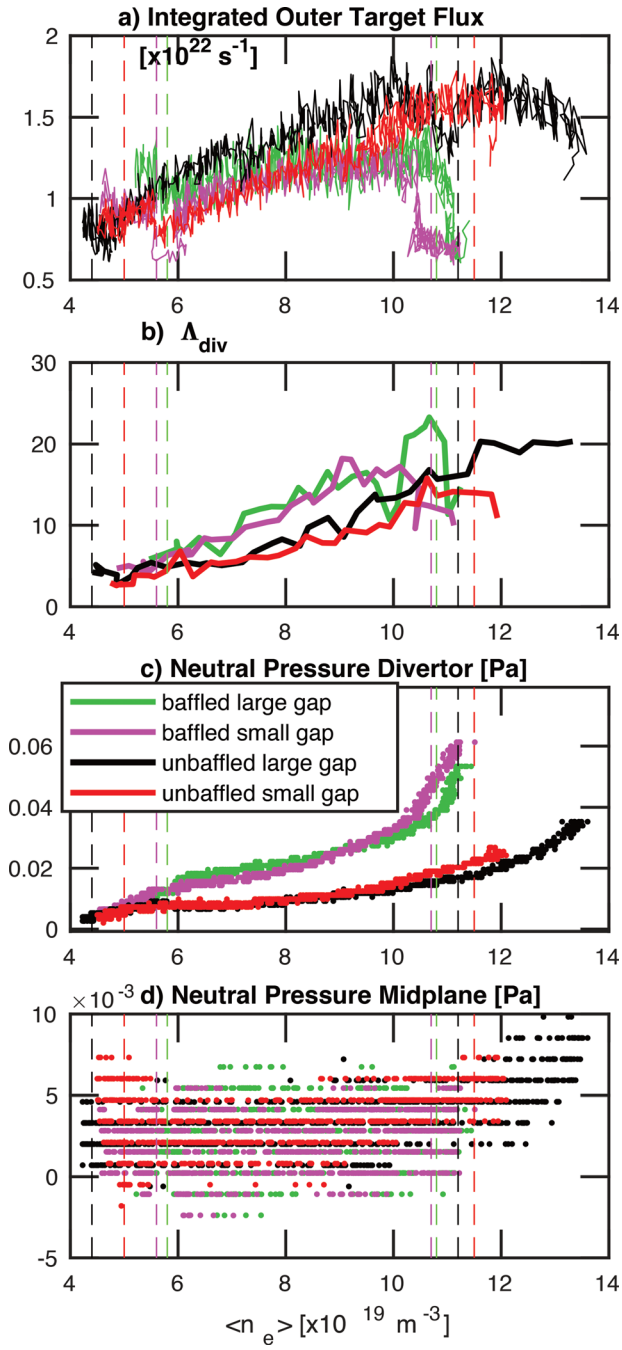

FIG. 2. The evolution of (a) the integrated particle flux to the outer target, (b) the normalized divertor collisionality Λ_{div}, and (c) the neutral pressure measured in the divertor and (d) the main-chamber, as functions of line averaged density $\langle n_e \rangle$. Vertical dashed lines show the $\langle n_e \rangle$ of the reciprocating probe plunges.

simulations.[35–37] The main-chamber neutral pressure gauge is below the noise floor [Fig. 2(d)] and cannot be used to directly verify the changes to the main-chamber neutral pressure.[34] [Note that each point represents an individual reading from the pressure gauge, where the vertical scatter is a result of the "noise floor" of the gauge and its electronics. Some values are negative because the pressure is equal to zero within the gauge's uncertainty. The discrete spacing in the pressure values show the quantization noise of the digitizer (i.e., rounding to the nearest bit).]

However, three independently run simulations using SOLPS-ITER[35,36] and SOLEDGE2D-Eirene[37] show that the baffles reduce neutral pressure in the main chamber by a factor of 2–5× over a wide range of $\langle n_e \rangle$ and input power. Even in simulations where the baffles were intentionally too short (poor divertor closure) or too long (increasing the recycling on top of the baffle), the main-chamber neutral pressure was still reduced by at least 2× compared to the unbaffled simulations.[37]

Baffled plasmas also feature higher CIII fronts, more divertor radiation, and inner target I_{sat} rollover,[33,34] while simulations show a 3–10× increase in divertor Balmer-alpha emission.[36]

Reciprocating probe plunges were taken at low $\langle n_e \rangle = 5.1 \pm 0.7\,(\times 10^{19}\,\mathrm{m}^{-3})$ and high $\langle n_e \rangle = 11.1 \pm 0.4\,(\times 10^{19}\,\mathrm{m}^{-3})$ in each scenario as represented by the vertical dashed lines in Fig. 2.

At first glance, the divertor conditions suggest that the baffled scenarios should have higher density shoulder amplitudes since they have higher Λ_{div} (associated with increased filamentary transport) and lower outer target flux (which is related to the density sink via parallel drainage). In Sec. IV, we will show that the opposite is true.

IV. DENSITY SHOULDER DEPENDENCE ON MAIN-CHAMBER NEUTRALS

The SOL density profiles at the midplane are compared between the four scenarios in Fig. 3. The location of the separatrix (dashed vertical line) has uncertainties of ±3 mm, shown by the shaded region. The low $\langle n_e \rangle$ density profiles (lines) match within measurement uncertainty for all four scenarios. A small but non-negligible shoulder is observed in the low $\langle n_e \rangle$ density profiles, i.e., the density decay length in the far-SOL ($\lambda_{ne,far} = 2.7 \pm 1.2$ cm) is longer than in the

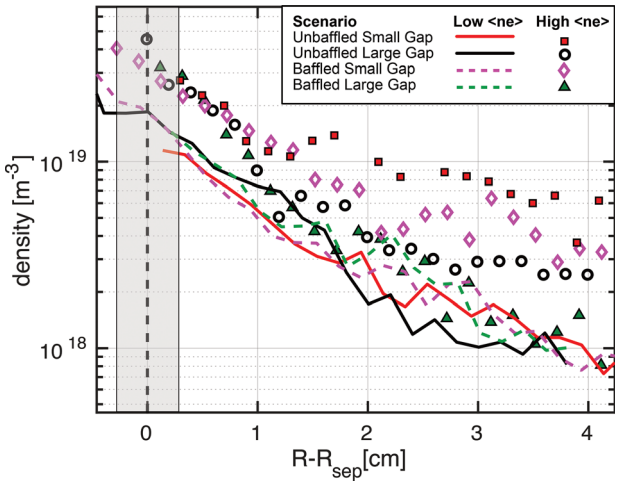

FIG. 3. Density profiles measured low $\langle n_e \rangle = 5.1 \pm 0.7\,(\times 10^{19}\,\mathrm{m}^{-3})$ (lines—unbaffled, dashed lines—baffled) and high $\langle n_e \rangle = 11.1 \pm 0.4\,(\times 10^{19}\,\mathrm{m}^{-3})$ (markers) for each scenario (see legend). The shaded region indicates the ± 3 mm uncertainty in the location of the separatrix.

near-SOL ($\lambda_{ne,near} = 0.9 \pm 0.2$ cm). At R-$R_{sep} > 2.7$ cm, the flux surfaces of the baffled scenarios (dashed lines) intersect with the outer baffle, but this does not cause a change in the profiles which continue to agree with the unbaffled profiles (solid lines).

We define a simple density shoulder amplitude

$$A_{s,4} = \frac{n_e(R - R_{sep} = 4\text{cm})}{n_e(R - R_{sep} = 0)}, \tag{3}$$

where the low $\langle n_e \rangle$ profiles have $A_{s,4} \sim 0.05$. The choice to consider n_e at R-$R_{sep} = 4$ cm is arbitrary. We found that this definition reduced the scatter compared to other definitions of shoulder amplitude,[22,23] especially at intermediate values of $\langle n_e \rangle$.

Comparing the baffled large gap scenario at low and high $\langle n_e \rangle$ (Fig. 3, green dashed line vs green triangles) shows no density shoulder broadening, with a small reduction in $A_{s,4}$ from 0.05 to 0.04. Relative to this case (green triangles) the density shoulder amplitude is increased by either removing the baffles (black circles, $A_{s,4} = 0.07$) or reducing the inner wall gap (magenta diamonds, $A_{s,4} = 0.10$). The effects appear to be cumulative as the scenario without baffles and with small gaps (red squares) has the strongest density shoulder with $A_{s,4} = 0.16$.

$A_{s,4}$ is plotted as a function of $\langle n_e \rangle$ for the expanded dataset in Fig. 4. The large symbols show $A_{s,4}$ for the profiles in Fig. 3, including the two black and magenta datapoints. $A_{s,4}$ remains constant across the range of $\langle n_e \rangle$ for the baffled large gap dataset (green triangles), i.e., density shoulder broadening does not occur even at the density limit in detached conditions. In contrast, the unbaffled small gap dataset (red squares) shows typical density shoulder evolution where $A_{s,4}$ increases with $\langle n_e \rangle$.

$\lambda_{ne,near} \sim 0.8 \pm 0.3$ cm and $\lambda_{ne,far} \sim 3.5 \pm 1.0$ cm remain roughly constant across the dataset, while the transition point between the steep $\lambda_{ne,near}$ and shallow $\lambda_{ne,far}$ regions move inward with increasing $A_{s,4}$. It is coincidental that some of the λ_{ne} transition points in Fig. 3 correspond with flux surfaces that intercept parts of the main chamber.

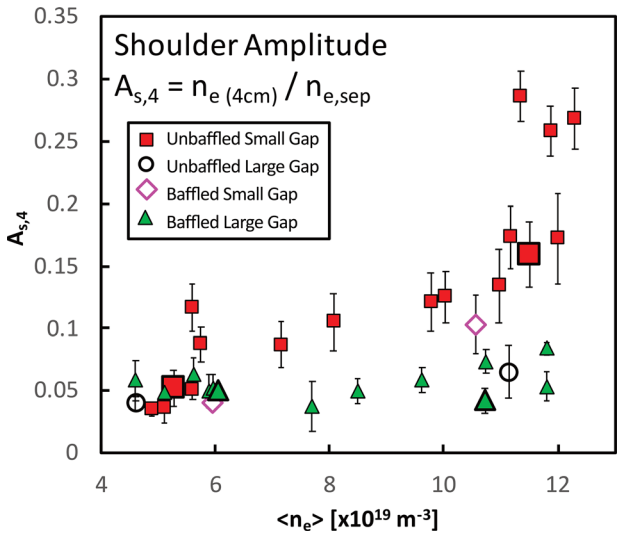

FIG. 4. Shoulder amplitude as a function of $\langle n_e \rangle$ for each scenario (see legend). The larger symbols represent the density profiles from Fig. 3.

In summary, density shoulder broadening does not occur in discharges, where the main-chamber neutral pressure is minimized using baffles and a wide inner wall gap. Removing the baffles or decreasing the inner gap both act to increase $A_{s,4}$, which varies by 4× across otherwise identical discharges.

V. CORRELATION BETWEEN TURBULENCE AND DENSITY SHOULDER AMPLITUDE

The turbulent transport characteristics are compared between the four scenarios at high $\langle n_e \rangle$, i.e., for identical discharges except for the different density shoulder amplitudes and differences in main-chamber neutral sources. These data are plotted up until the first electrode arc and thus are not available at or inside the separatrix.

Γ_r^{turb} [Fig. 5(a)] is ∼2× higher for the unbaffled small gap scenario (red squares) where the density shoulder is strongest than the other three scenarios. The elevated Γ_r^{turb} mainly results from an increase in density fluctuations [see Fig. 5(b) where the Isat RMS magnitude $\langle \tilde{I}_{sat}^2 \rangle^{1/2}$ is taken as a proxy for $\langle \tilde{n}_e^2 \rangle^{1/2}$ as it requires fewer assumptions and has less scatter]. Γ_r^{turb} and $\langle \tilde{I}_{sat}^2 \rangle^{1/2}$ agree for the other three scenarios within their scatter.

Γ_r^{turb} is plotted for the expanded dataset in Fig. 6 as a function of the shoulder amplitude. The averaging interval for Γ_r^{turb} [see Eq. (1)] is taken over 2 cm < R−R_{sep} < 3 cm to provide a comparable outer-

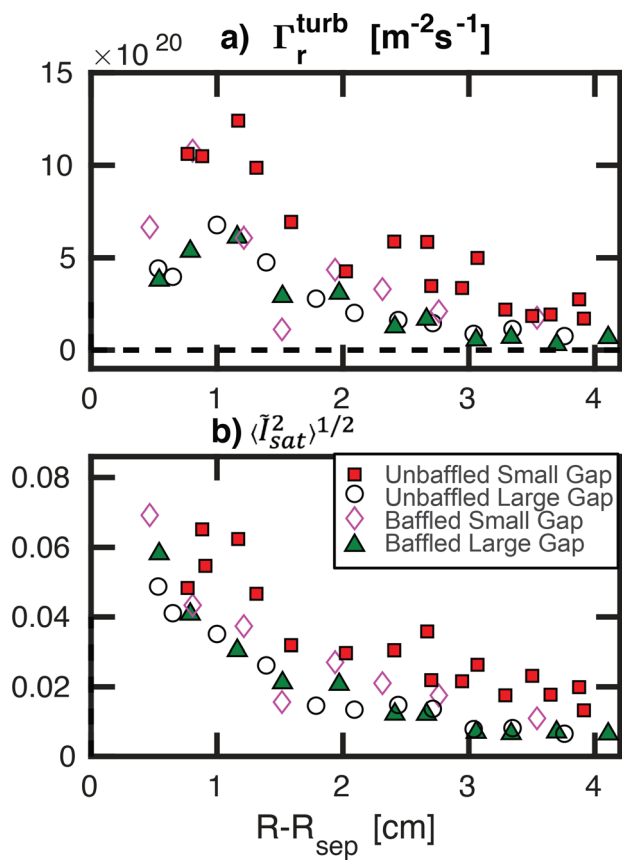

FIG. 5. The radial turbulent flux (a) and the RMS level of the ion saturation current (b) for the four scenarios at high line average density.

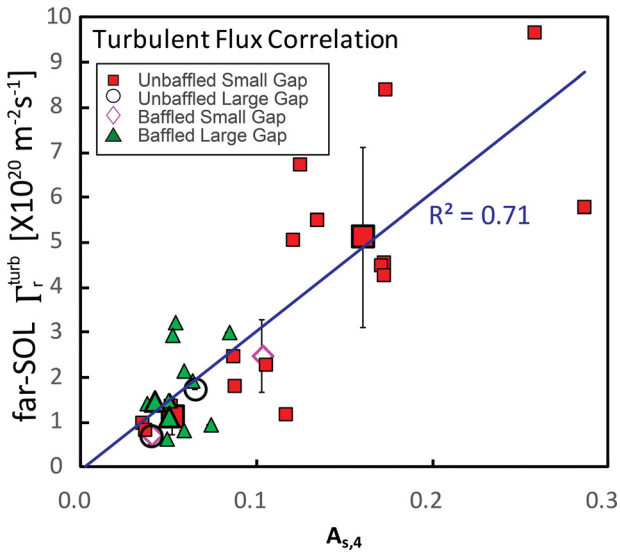

FIG. 6. The radial turbulent flux averaged over 2 cm < R-R_{sep} < 3 cm as a function of density shoulder amplitude. Example error bars are shown for select datapoints, representing the scatter in the data. The larger symbols represent the density profiles from Fig. 3. The line is a linear fit to all datapoints ($y = 3.1 \times 10^{21} \times - 5.7 \times 10^{18}$).

SOL flux for each probe plunge. The solid line is a linear fit to all datapoints and shows that Γ_r^{turb} correlates strongly with $A_{s,4}$. For the baffled large gap scenario (green triangles) with no shoulder broadening, Γ_r^{turb} remains ~constant across the range of $\langle n_e \rangle$ up to the density limit. The shoulder amplitude $A_{s,4}$ increases with Γ_r^{turb}, not with $\langle n_e \rangle$.

VI. DISCUSSION

Baffled discharges feature higher divertor neutral pressure, colder denser more collisional plasmas, and earlier onset of detachment, i.e., conditions which are associated with higher turbulent transport thought to drive density shoulder broadening. However, the baffled large gap dataset has no shoulder broadening and low turbulent transport. This shows that unknown parameter in addition to Λ_{div} are important in setting the radial turbulent flux, with multiple candidates under investigation.[25–27] A strong correlation is observed between the shoulder amplitude and radial turbulent flux. The baffled scenarios show that turbulent flux does not necessarily increase with $\langle n_e \rangle$, with Λ_{div}, or with the degree of detachment.

The baffled discharges feature reduced outer target ion flux. The target flux is related to, but not equal to the sink term for the upstream SOL density. The parallel and poloidal fluxes vary along the fieldline because of ionization throughout the divertor,[41] and the inner divertor must be considered as well. The presence of the baffles reduces the shoulder amplitude while also reducing the outer target flux, but a more detailed investigation is needed to test the importance of the sink term on the density shoulder.

VII. CONCLUSIONS

Density shoulder broadening does not occur in baffled discharges with large inner gaps, i.e., when the sources of main-chamber neutrals are minimized. Removing the baffles reduces divertor closure and increases the density shoulder amplitude. Reducing the inner wall gap increases the source of recycling neutrals in the main-chamber and also increases the shoulder amplitude. These two effects are cumulative, and the shoulder amplitude is further increased when the small gap and lack of baffles are used together. Modifying the sources of main-chamber neutrals causes a 4× difference in shoulder amplitude in otherwise identical discharges. These results are consistent with the hypothesis that high main-chamber neutral density is required for density shoulder broadening. Radial turbulent flux correlates with shoulder amplitude, which is mainly a result of an increased I_{sat} RMS level.

These results indicate that density shoulder growth may be preventable in future tokamaks by designing for good divertor neutral closure and by minimizing main-chamber neutral sources. Since the baseline ITER scenarios feature pellet fueling, good divertor closure, and wide gaps to the walls with a minimum R-R_{sep} = 4 cm,[42] main-chamber neutral pressures should be low, and the conditions necessary for shoulder broadening may not be present; however, further study is required to verify if these findings extend to ITER relevant H-mode conditions.

ACKNOWLEDGMENTS

This work was supported by the U.S. Department of Energy under Grant No. DE-SC0010529 and by the Swiss National Science Foundation. This work has been carried out within the framework of the EUROfusion Consortium and has received funding from the Euratom Research and Training Programme 2014–2018 and 2019–2020 under Grant Agreement No 633053. The views and opinions expressed herein do not necessarily reflect those of the European Commission. The technical contributions of L. Chousal and C. Jones are gratefully acknowledged.

AUTHOR DECLARATIONS

Conflict of Interest

The authors have no conflicts to disclose.

DATA AVAILABILITY

The data that support the findings of this study are available within the article.

REFERENCES

[1] K. McCormick, G. Kyriakakis, J. Neuhauser, E. Kakoulidis, J. Schweinzer, and N. Tsois, "Particle and energy transport scalings in the ASDEX scrape-off layer," J. Nucl. Mater. **196–198**, 264–270 (1992).
[2] B. LaBombard, R. L. Boivin, M. Greenwald, J. Hughes, B. Lipschultz, D. Mossessian, C. S. Pitcher, J. L. Terry, and S. J. Zweben, "Particle transport in the scrape-off layer and its relationship to discharge density limit in Alcator C-Mod," Phys. Plasmas **8**, 2107–2117 (2001).
[3] O. E. Garcia, R. A. Pitts, J. Horacek, A. H. Nielsen, W. Fundamenski, J. P. Graves, V. Naulin, and J. J. Rasmussen, "Turbulent transport in the TCV SOL," J. Nucl. Mater. **363–365**, 575–580 (2007).
[4] D. L. Rudakov, J. A. Boedo, R. A. Moyer, S. Krasheninnikov, A. W. Leonard, M. A. Mahdavi, G. R. McKee, G. D. Porter, P. C. Stangeby, J. G. Watkins *et al.*, "Fluctuation-driven transport in the DIII-D boundary," Plasma Phys. Controlled Fusion **44**, 717–731 (2002).
[5] A. Zito, M. Wischmeier, D. Carralero, P. Manz, I. Paradela Pérez, M. Passoni, and T. T. ASDEX Upgrade, "Numerical modelling of an enhanced

perpendicular transport regime in the scrape-off layer of ASDEX Upgrade," Plasma Phys. Controlled Fusion **63**, 75003 (2021).
[6]P. C. Stangeby, "Modeling plasma contact with the main vessel walls of a divertor tokamak," Phys. Plasmas **9**, 3489 (2002).
[7]D. Carralero, G. Birkenmeier, H. W. W. Müller, P. Manz, P. deMarne, S. H. H. Müller, F. Reimold, U. Stroth, M. Wischmeier, and E. Wolfrum, "An experimental investigation of the high density transition of the scrape-off layer transport in ASDEX Upgrade," Nucl. Fusion **54**, 123005 (2014).
[8]D. Carralero, P. Manz, L. Aho-Mantila, G. Birkenmeier, M. Brix, M. Groth, H. W. Müller, U. Stroth, N. Vianello, and E. Wolfrum, "Experimental validation of a filament transport model in turbulent magnetized plasmas," Phys. Rev. Lett. **115**, 215002 (2015).
[9]D. L. Rudakov, J. A. Boedo, R. A. Moyer, P. C. Stangeby, J. G. Watkins, D. G. Whyte, L. Zeng, N. H. Brooks, R. P. Doerner, T. E. Evans *et al.*, "Far SOL transport and main wall plasma interaction in DIII-D," Nucl. Fusion **45**, 1589–1599 (2005).
[10]O. E. Garcia, J. Horacek, R. A. Pitts, A. H. Nielsen, W. Fundamenski, V. Naulin, and J. J. Rasmussen, "Fluctuations and transport in the TCV scrape-off layer," Nucl. Fusion **47**, 667–676 (2007).
[11]D. A. Russell, J. R. Myra, and D. A. D'Ippolito, "Collisionality and magnetic geometry effects on tokamak edge turbulent transport. II. Many-blob turbulence in the two-region model," Phys. Plasmas **14**, 102307 (2007).
[12]F. Militello and J. T. Omotani, "Scrape Off Layer profiles interpreted with filament dynamics," Nucl. Fusion **56**, 104004 (2016).
[13]C. F. Beadle and P. Ricci, "Understanding the turbulent mechanisms setting the density decay length in the tokamak scrape-off layer," J. Plasma Phys. **86**, 175860101 (2020).
[14]N. Vianello, C. K. Tsui, C. Theiler, S. Allan, J. Boedo, B. Labit, H. Reimerdes, K. Verhaegh, W. A. J. Vijvers, N. Walkden *et al.*, "Modification of SOL profiles and fluctuations with line-average density and divertor flux expansion in TCV," Nucl. Fusion **57**, 116014 (2017).
[15]M. Giacomin, A. Stagni, P. Ricci, J. A. Boedo, J. Horacek, H. Reimerdes, and C. K. Tsui, "Theory-based scaling laws of near and far scrape-off layer widths in single-null L-mode discharges," Nucl. Fusion **61**, 076002 (2021).
[16]D. Carralero, M. Siccinio, M. Komm, S. A. Artene, F. A. D'Isa, J. Adamek, L. Aho-Mantila, G. Birkenmeier, M. Brix, G. Fuchert *et al.*, "Recent progress towards a quantitative description of filamentary SOL transport," Nucl. Fusion **57**, 056044 (2017).
[17]N. Vianello, D. Carralero, C. K.-W. Tsui, V. Naulin, M. Agostini, I. Cziegler, B. Labit, C. Theiler, E. Wolfrum, D. Aguiam *et al.*, "Scrape-off layer transport and filament characteristics in high-density tokamak regimes," Nucl. Fusion **60**, 016001 (2020).
[18]F. Militello, L. Garzotti, J. Harrison, J. T. Omotani, R. Scannell, S. Allan, A. Kirk, I. Lupelli, A. J. Thornton, and the MAST Team, "Characterisation of the L-mode scrape off layer in MAST: Decay lengths," Nucl. Fusion **56**, 16006 (2016).
[19]D. A. D'Ippolito and J. R. Myra, "Thermal transport catastrophe and the tokamak edge density limit," Phys. Plasmas **13**, 062503 (2006).
[20]J. R. Myra, D. A. D'Ippolito, D. P. Stotler, S. J. Zweben, B. P. Leblanc, J. E. Menard, R. J. Maqueda, J. Boedo, D. A. D 'ippolito, D. P. Stotler *et al.*, "Blob birth and transport in the tokamak edge plasma: Analysis of imaging data," Phys. Plasmas **13**, 092509 (2006).
[21]D. Carralero, J. Madsen, S. A. Artene, M. Bernert, G. Birkenmeier, T. Eich, G. Fuchert, F. Laggner, V. Naulin, P. Manz *et al.*, "A study on the density shoulder formation in the SOL of H-mode plasmas," Nucl. Mater. Energy **12**, 1189–1193 (2017).
[22]A. Wynn, B. Lipschultz, I. Cziegler, J. Harrison, A. Jaervinen, G. F. Matthews, J. Schmitz, B. Tal, M. Brix, C. Guillemaut *et al.*, "Investigation into the formation of the scrape-off layer density shoulder in JET ITER-like wall L-mode and H-mode plasmas," Nucl. Fusion **58**, 056001 (2018).
[23]O. Février, C. Theiler, J. R. Harrison, C. K. Tsui, K. Verhaegh, C. Wüthrich, J. A. Boedo, H. De Oliveira, B. P. Duval, B. Labit *et al.*, "Nitrogen-seeded divertor detachment in TCV L-mode plasmas," Plasma Phys. Controlled Fusion **62**, 035017 (2020).
[24]M. Agostini, N. Vianello, L. Carraro, D. Carralero, M. Cavedon, R. Dux, V. Naulin, M. Spolaore, and E. Wolfrum, "Neutral density estimation in the ASDEX upgrade divertor from deuterium emissivity measurements during detachment and shoulder formation," Plasma Phys. Controlled Fusion **61**, 115001 (2019).
[25]Y. Zhang and S. I. Krasheninnikov, "Effect of neutrals on the anomalous edge plasma transport," Plasma Phys. Controlled Fusion **62**, 115018 (2020).
[26]D. A. D'Ippolito, J. R. Myra, and S. I. Krasheninnikov, "Cross-field blob transport in tokamak scrape-off-layer plasmas," Phys. Plasmas **9**, 222 (2002).
[27]A. S. Thrysøe, V. Naulin, A. H. Nielsen, and J. Juul Rasmussen, "Dynamics of seeded blobs under the influence of inelastic neutral interactions," Phys. Plasmas **27**, 052302 (2020).
[28]D. Mancini, P. Ricci, N. Vianello, M. Giacomin, and A. Coroado, "Investigation of the density shoulder formation by using self-consistent simulations of plasma turbulence and neutral kinetic dynamics," Nucl. Fusion **61**, 126029 (2021).
[29]H. Reimerdes, S. Alberti, P. Blanchard, P. Bruzzone, R. Chavan, S. Coda, B. P. P. Duval, A. Fasoli, B. Labit, B. Lipschultz *et al.*, "TCV divertor upgrade for alternative magnetic configurations," Nucl. Mater. Energy **12**, 1106–1111 (2017).
[30]A. Fasoli, "TCV heating and in-vessel upgrades for addressing DEMO physics issues," Nucl. Fusion **55**, 043006 (2015).
[31]C. K. Tsui, J. A. Boedo, P. C. Stangeby, and the TCV Team, "Accounting for Debye sheath expansion for proud Langmuir probes in magnetic confinement fusion plasmas," Rev. Sci. Instrum. **89**, 013505 (2018).
[32]P. C. Liewer, "Measurements of microturbulence in tokamaks and comparisons with theories of turbulence and anomalous transport," Nucl. Fusion **25**, 543–621 (1985).
[33]O. Février, H. Reimerdes, C. Theiler, D. Brida, C. Colandrea, B. P. Duval, H. De Oliveira, D. Galassi, S. Gorno, S. Henderson *et al.*, "Divertor closure effects on the TCV boundary plasma," Nucl. Mater. Energy **27**, 100977 (2021).
[34]H. Reimerdes, B. P. Duval, H. Elaian, A. Fasoli, O. Février, C. Theiler, F. Bagnato, M. Baquero-Ruiz, P. Blanchard, D. Brida *et al.*, "Initial TCV operation with a baffled divertor," Nucl. Fusion **61**, 024002 (2021).
[35]A. Fasoli, H. Reimerdes, S. Alberti, M. Baquero-Ruiz, B. P. Duval, E. Havlikova, A. Karpushov, J. M. Moret, M. Toussaint, H. Elaian *et al.*, "TCV heating and divertor upgrades," Nucl. Fusion **60**, 016019 (2020).
[36]M. Wensing, B. P. Duval, O. Février, A. Fil, D. Galassi, E. Havlickova, A. Perek, H. Reimerdes, C. Theiler, K. Verhaegh *et al.*, "SOLPS-ITER simulations of the TCV divertor upgrade," Plasma Phys. Controlled Fusion **61**, 085029 (2019).
[37]D. Galassi, H. Reimerdes, C. Theiler, M. Wensing, H. Bufferand, G. Ciraolo, P. Innocente, Y. Marandet, and P. Tamain, "Numerical investigation of optimal divertor gas baffle closure on TCV," Plasma Phys. Controlled Fusion **62**, 115009 (2020).
[38]A. Fil, B. Lipschultz, D. Moulton, B. D. Dudson, O. Février, O. Myatra, C. Theiler, K. Verhaegh, and M. Wensing, "Separating the roles of magnetic topology and neutral trapping in modifying the detachment threshold for TCV," Plasma Phys. Controlled Fusion **62**, 035008 (2020).
[39]O. Février, C. Theiler, H. De Oliveira, B. Labit, N. Fedorczak, and A. Baillod, "Analysis of wall-embedded Langmuir probe signals in different conditions on the tokamak à configuration variable," Rev. Sci. Instrum. **89**, 053502 (2018).
[40]H. De Oliveira, P. Marmillod, C. Theiler, R. Chavan, O. Février, B. Labit, P. Lavanchy, B. Marlétaz, R. A. Pitts, and T. team, "Langmuir probe electronics upgrade on the tokamak à configuration variable," Rev. Sci. Instrum. **90**, 083502 (2019).
[41]H. D. Oliveira, C. Theiler, H. Reimerdes, B. Duval, C. Tsui, S. Gorno, and A. Perek, "New insights on divertor parallel flows, E×B drifts, and fluctuations from *in situ*, two-dimensional probe measurement in the tokamak à configuration variable," Nucl. Fusion (submitted).
[42]R. A. Pitts, S. Carpentier, F. Escourbiac, T. Hirai, V. Komarov, A. S. Kukushkin, S. Lisgo, A. Loarte, M. Merola, R. Mitteau *et al.*, "Physics basis and design of the ITER plasma-facing components," J. Nucl. Mater. **415**, S957–64 (2011).